Geophysical Journal International

Geophys. J. Int. (2011) **186,** 1380–1388 doi: 10.1111/j.1365-246X.2011.05118.x

Analysis of the crustal thickness and Poisson's ratio in eastern Tibet from teleseismic receiver functions

Haiyan Yang, Jiafu Hu, Guangquan Li, Hong Zhao and Limin Wen

Department of Geophysics, Yunnan University, 2 North Green Lake Rd., Kunming, Yunnan 650091, *P. R. China. E-mail: guangquanli74@gmail.com*

Accepted 2011 June 18. Received 2011 May 21; in original form 2010 August 6

SUMMARY

Crustal thickness and Poisson's ratio are two key parameters for investigating tectonic setting and evolution. The *H-k* technique has become popular to determinate their values in recent years. However, if a complex structure exists in the crust, the reverberated phases from different depths may interfere with each other, resulting in reduction or even absence of the *PpPs* phase from the Moho, such that the *H-k* algorithm may not reveal unambiguous estimates of these two parameters. In this paper, the *H-k* technique is applied to process a synthetic receiver function for a test case, the result of which is compared with that from direct picking of the time delays of the converted and reverberated phases. Then we process the observational data recorded at two stations in eastern Tibet, determine the crustal thickness and the velocity ratio using the two methods, compare the result with that obtained by Xu *et al*. at the same location, and analyse the potential causes for discrepancy as well as the reliability of the two methods. Finally, the crustal thickness and the Poisson's ratio in eastern Tibet and Sichuan Basin are determined from the receiver functions recorded at 51 broad-band stations, using the two different methods. The results indicate that the crustal thickness from the time delays is thicker than that from the *H-k* algorithm near the eastern Himalayan syntaxis, and the crustal Poisson's ratio in the rigid Sichuan Basin from the time delays ranges from 0.26 to 0.28, which are more reasonable than that from the *H-k* (0.28 to 0.34). Additionally, the Poisson's ratio under the faults from the time delays is found to be higher than those on the two sides, which is consistent with the tectonic background and previous study.

Key words: Composition of the continental crust; Body waves; Asia.

1 INTRODUCTION

Depth of the Moho discontinuity and physical properties of enveloping rocks are important lithospheric parameters to evaluate accurately, as their spatial variations and absolute values can be related to tectonic evolution of the lithosphere. This paper focuses on the ability to constrain estimates of crustal thickness and Poisson's ratio (an elastic parameter that quantifies the shearing of a rock). Poisson's ratio for common rocks varies between 0.20 and 0.35, depending on their mineral composition (Zandt & Ammon 1995). The ratio decreases with silica content, but increases with mafic content. Poisson's ratio is often determined from the ratio of *P* and *S* wave velocities (V_p and V_s). Therefore, to determine as accurately as possible the V_p/V_s ratio can help us constrain the composition of the crust.

The *P* waveform of a teleseismic event contains significant information, including the focal time function, the near-source structure and the *Ps* and reverberation phases generated at the velocity interfaces within the crust and upper mantle. Based on the assumption of source equalization, the far-field path and the source effect can be removed effectively by deconvolving the vertical components from the radial components (Langston 1979; Gurrola *et al*. 1995; Bostock 1998). Thus the resulting receiver function provides an estimate of the impulse response on the ground.

Receiver functions can constrain velocity structure in crust and upper mantle through the relative amplitudes of the direct and converted waves, and can constrain depths of the interfaces through their relative traveltimes (Ammon *et al*. 1990). Over last few decades, the receiver function technology has become a standard tool to investigate crust and mantle structure (e.g. Bostock *et al*. 2002; Kind *et al*. 2002). The interpretation of the depth of a discontinuity mainly relies on the time delay between the converted phase generated at the discontinuity and the direct wave. To date, two methods are used to estimate crustal depth and V_p/V_s ratio in crust. The first is to identify the phases in a receiver function and pick up the time delays between the converted phases and the direct *P*, and the crustal depth and V_p/V_s ratio can then be computed from the time delays directly. The second is called the *H-k* stacking algorithm, developed by Zhu & Kanamori (2000). This algorithm does not require manual picking of the time delays of the converted

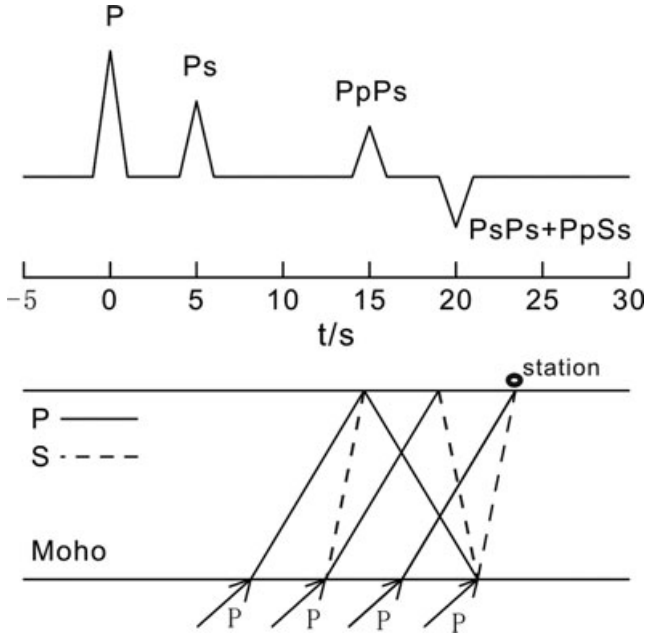

Figure 1. The ray paths of the direct, converted and reverberated phases generated at the Moho and a schematic representation of the receiver function.

phases in the receiver function, making it fast and efficient, and therefore, is widely adopted by seismologists to investigate depth of crust and V_p/V_s ratio in crust.

This paper aims to assess the pros and cons of the two methods in computing crustal thickness and V_p/V_s ratio in a region with complex tectonics. First, we design a special velocity model and synthesize a radial receiver function, in which the *PLs* phase from the lithosphere–asthenosphere boundary (LAB) reaches simultaneously with the *PpPs* phase from the Moho. The aforementioned two techniques are then applied to obtain the depth of the Moho and the V_p/V_s ratio. Second, as two practical examples, the broad-band waveforms recorded at two stations located near the Longmenshan (LMS) Fault that separates eastern Tibet from Sichuan Basin are processed. The geological structure of the LMS is very complex due to significant crustal shortening during the Mesozoic and to recent active tectonics related to the collision between the Indian subcontinent and the Eurasian continent (Wang & Burchfiel 2000). Our result is compared with that obtained by Xu *et al*. (2007), and the cause for discrepancy is explained. Finally, the contour maps of the Moho depth and the crustal Poisson's ratio in eastern Tibet and Sichuan Basin from the two different methods are compared and their reasonability is analysed.

2 METHOD AND SYNTHETIC EXAMPLE

As shown in Fig. 1, where the Moho is the deepest interface, the crustal thickness, H, can be expressed by the time delay, $t_{Ps} - t_P$ between the *Ps* phase and the direct *P* as follows (Zandt *et al*. 1995):

$$H = \frac{t_{Ps} - t_P}{\sqrt{V_s^{-2} - p^2} - \sqrt{V_p^{-2} - p^2}}, \tag{1}$$

where p is ray parameter, and V_p and V_s are velocities of *P* and *S* waves in crust, respectively. Similarly the time delay $t_{PpPs} - t_P$ between the multiple phase *PpPs* and the converted phase *Ps* can be expressed as

$$H = \frac{t_{PpPs} - t_{Ps}}{2\sqrt{V_p^{-2} - p^2}}. \tag{2}$$

The distance from a station sampled by a receiver function depends how far back the signal is and how deep the velocity interface lies. For a teleseismic event, the horizontal offset from the station is not large, because the Moho is shallow and thus the converted locations of phases (*P*, *Ps*, *PsPs* and *PpPs*) are close to the station (thus the sampled area could be assumed to be uniform). Also, the *P* waves incident to the Moho interface have a uniform incidence angle, so that the direct, converted and reverberated phases have a uniform ray parameter. For these reasons, we approximately have

$$t_{PsPs} - t_{PpPs} = t_{Ps} - t_P. \tag{3}$$

From eqs (1) and (2), we obtain the following equation:

$$\frac{t_{PpPs} - t_P}{t_{Ps} - t_P} = 1 + \frac{2\sqrt{V_p^{-2} - p^2}}{\sqrt{V_s^{-2} - p^2} - \sqrt{V_p^{-2} - p^2}}. \tag{4}$$

Since the ray parameter p is a smaller quantity close to zero. According to Taylor expansion to the second order,

$$\sqrt{V_p^{-2} - p^2} \approx V_p^{-1}\left[1 - \frac{V_p^2 p^2}{2}\right]$$

$$\sqrt{V_s^{-2} - p^2} \approx V_s^{-1}\left[1 - \frac{V_s^2 p^2}{2}\right].$$

For an epicentral distance of 67°, p is only at 0.057 s km^{-1}. With $V_p = 6.5$ km s^{-1}, $V_p^2 p^2/2$ is only 0.07 and $V_s^2 p^2/2$ is even smaller, such that eq. (4) can be approximated as

$$\frac{t_{PpPs} - t_P}{t_{Ps} - t_P} \approx 1 + \frac{2}{\frac{V_p}{V_s} - 1}.$$

Typically, the average value of the V_p/V_s ratio ranges from 1.732 to 2.0 for crustal rocks, and therefore,

$$\frac{t_{PpPs} - t_P}{t_{Ps} - t_P} \approx 3.58 \sim 3.00. \tag{5}$$

Substituting (3) into (5) yields

$$\frac{t_{PsPs} - t_P}{t_{Ps} - t_P} \approx 1 + (3.58 \sim 3.00). \tag{6}$$

Eqs (5) and (6) provide a clue to identifying the reverberation phases in the stacked receiver function with an epicentral distance of 67°. Once a converted phase is found, it becomes possible to predict the time delays of the multiple phases, and vice versa. Please note that eqs (5) and (6) are no for recognizing the phases on individual traces. Now dividing (1) by (2) and taking squares on both sides of the resulting equation, the velocity ratio can be accurately calculated as (Zandt *et al*. 1995)

$$\frac{V_p}{V_s} = \left\{(1 - p^2 V_p^2)\left[2\left(\frac{t_{Ps} - t_P}{t_{PpPs} - t_{Ps}}\right) + 1\right]^2 + p^2 V_p^2\right\}^{1/2}. \tag{7}$$

Substituting (3) into (7) yields

$$\frac{V_p}{V_s} = \left\{(1 - p^2 V_p^2)\left[2\left(\frac{t_{Ps} - t_P}{t_{PsPs} - 2t_{Ps} + t_P}\right) + 1\right]^2 + p^2 V_p^2\right\}^{1/2}. \tag{8}$$

Table 1. The designed velocity model.

No. of layer	Thickness (km)	V_p (km s^{-1})	V_s (km s^{-1})	Density (g cm^{-3})	V_p/V_s
1	20	5.1962	3.0000	2.4328	1.732
2	15	6.5818	3.8000	2.8762	1.732
3	115	7.7942	4.5000	3.2642	1.732
4	Infinite	6.9282	4.0000	2.9870	1.732

Although the *P*-wave velocity is present on the right-hand sides of eqs (7) and (8), it has only a minor effect on the ratio V_p/V_s. According to a statistical study by Zandt *et al*. (1995), the global average velocity of *P* wave in crust ranges from 6.00 to 6.50 km s^{-1}. If the time delays are precisely measured, the value of V_p/V_s differs only by 0.05 when the largest and the smallest velocity values are applied. The value of the Poisson's ratio of crust is obtained once the velocity ratio is measured. The resulting Poisson's ratio varies by less than 0.02 (Zandt *et al*. 1995). Their study has indicated that determination of crustal thickness and V_p/V_s ratio using time delays is not sensitive to crustal *P* velocity, and for this reason, a *P*-wave velocity of 6.25 km s^{-1} is used in this paper. Once the time delays between the converted/reverberated phases and the direct *P* is obtained, the velocity ratio can be determined through eq. (7) or (8), and the crustal thickness can be obtained through eq. (1) or (2).

Crustal thickness H and velocity ratio k (V_p/V_s) can be estimated from the relative timings of conversion and reverberation. The differential traveltimes depend on H, k, the average crustal *P*-wave velocity and the ray parameter. The last two can be easily determined. For each receiver function, we follow the approach of Zhu & Kanamori (2000) and summarize the amplitudes of the receiver function at the predicted differing traveltimes of the *Ps*, *PpPs* and *PsPs* (or *PpSs*) phases.

$$S(H,k) = w_1 r(t_{Ps} - t_P) + w_2 r(t_{PpPs} - t_P) - w_3 r(t_{PsPs} - t_P), \quad (9)$$

where $w_1 = 0.7$, $w_2 = 0.2$ and $w_3 = 0.1$ are weighing factors. Given a pair of (H, k), the time delays can be computed from eqs (1)–(3). For each receiver function, we use eq. (9) to get an H-k surface with amplitude $S(H, k)$. Then these surfaces are superimposed to get a final solution surface. The optimum solution (H, k) is located at where the *S(H, k)* reaches the maximum value on the final surface. Generally, the *Ps* phase from the Moho is clearly visible in a receiver function, but the reverberation phases may be weak or even disappear due to lateral variation of the Moho and/or interference from an intracrust interface.

Table 1 lists the parameters for a velocity model, in which the depths of the Moho and the LAB are set to be 35 km and 150 km, respectively, and the crustal velocity ratio V_p/V_s is 1.732. We prescribe a ray parameter $p = 0.06$ s km^{-1}, apply a reflection matrix approach (Kennett 1983) to compute the seismic response on the ground, and obtain the receiver function by deconvolving the vertical component from the radial component. As shown in Fig. 2, the predicted traveltimes of the converted and reverberated phases are labelled. In this example, the *Phs* converted phase is from the intracrust interface, while the *PpPhs* and *PsPhs* phases are the reverberation phases from this interface. These phases are pretty visible, satisfying eqs (5) and (6). By searching over the H-k space, the optimum solution is found to be located at point (22.5, 1.818). This result from the H-k algorithm is associated with the intracrust layer in the designed model. Unfortunately, the amplitude associated with the Moho is too weak to identify, which illustrates that in this case, it is difficult to recognize the Moho.

On the other hand, we pick up the time delay of *Ps* phase to be 4.7 s; according to eqs (5) and (6), the *PpPs* and *PsPs* phases should appear approximately at 16 s and 20 s, respectively. Unfortunately, in the receiver function in Fig. 2, the *PpPs* phase from the Moho is too weak to identify. Nonetheless we can pick up the *PsPs* phase using eq. (6), whose delay is 20.8 s. Accordingly, the value of V_p/V_s computed from eq. (8) is 1.734, and the depth of the Moho from eq. (1) is 38.07 km. This result is close to what we prescribed, but significantly different from that determined from the H-k algorithm.

The cause for the discrepancy is that the negative *PLs* phase from the LAB lays over the reverberation phase *PpPs*, such that the maximum value stacked by the H-k algorithm does not appear at the correct position in the H-k space. In real cases, the interference between the Moho and intracrustal discontinuity, which are close to each other on the H-k space, may reduce the Moho multiple phase.

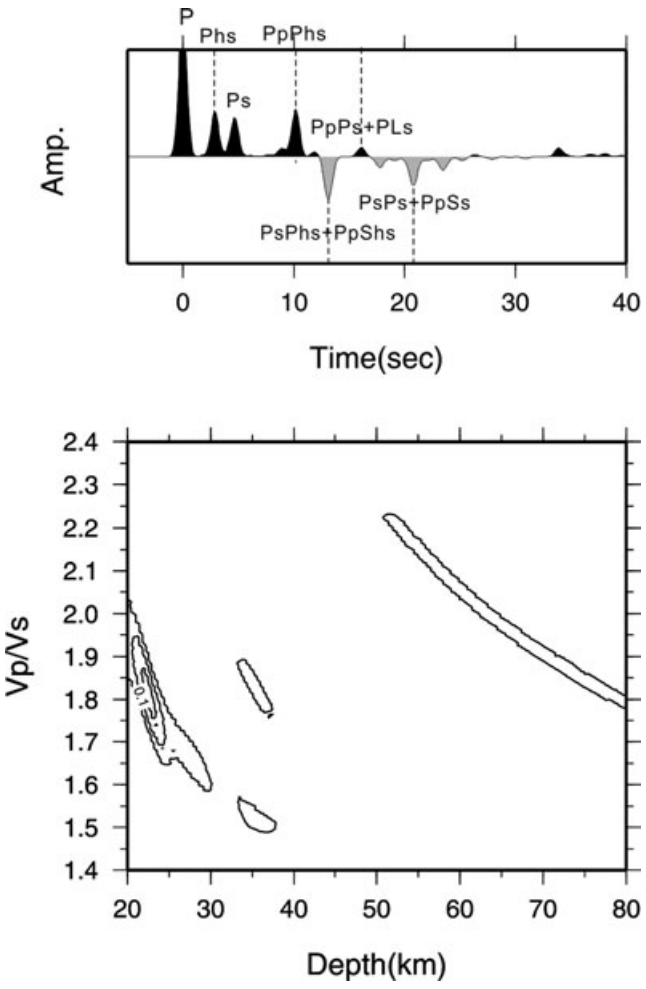

Figure 2. (a) The receiver function resulting from the designed velocity model, in which three phases *Ps*, *PpPs* and *PsPs* + *PpSs* are generated at the Moho, while the phases of *Phs*, *PpPhs* and *PsPhs* + *PpShs* are generated at the intracrust discontinuity. The *PLs* phase is a converted phase from the LAB. (b) The solution surface constructed by the H-k algorithm, with the contour intervals at 0.03.

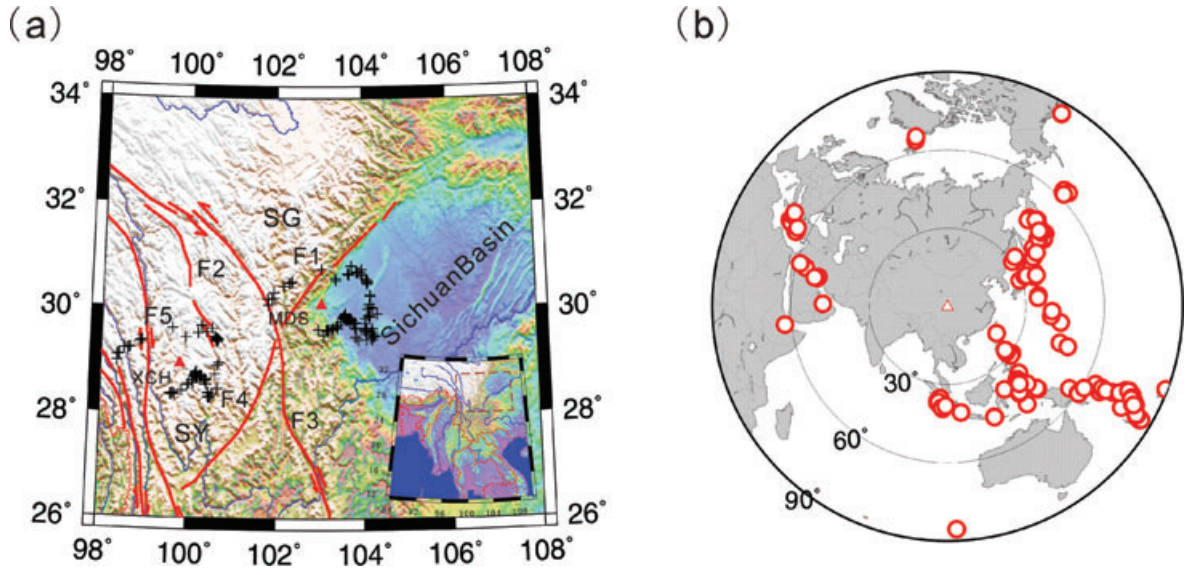

Figure 3. (a) Location of the seismic stations (triangles) and the piercing points at depth 300 km (crosses), sketch of the geological setting and topography of eastern Tibet. The regional faults: F1, Longmenshan Fault; F2, Xianshuihe–Anninghe Fault; F3, Lijiang–Jinhe Fault; F4, Xiaojinhe Fault; F5, Jinshajiang-Red River Fault. SG, Songpan–Ganze Fold; SY, Sichuan–Yunnan Block. (b) Distribution of the seismic events with epicentral distances from 0° to 90° (the azimuth projection centred around station MDS).

Additionally, the *PsPs* phase generated by an intracrust interface could reduce the *PpPs* phase generated by the Moho.

3 TWO EXAMPLES

The Tibetan Plateau is a result of the collision between the Indian Plate and the Eurasian Continent, which started approximately 50 Ma ago and has produced a convergence belt of 2000 km wide. GPS measurements have confirmed that crustal material is moving eastwards in eastern Tibet and obstructed by the rigid Sichuan Basin of the Yangtze Craton (Clark & Royden 2000; Copley & McKenzie 2007), as the velocity decreases in the east direction (Zhang *et al*., 2004). As shown in Fig. 3, the crustal motion of the Sichuan–Yunnan (SY) block, interpreted as a southeastward extrusion of crustal material from the Tibetan Plateau, is dominated by a clockwise rotation around the eastern Himalayan syntaxis, as revealed by geodetic measurements (King *et al*. 1997; Zhang *et al*. 2004) and geological studies (Wang & Burchfiel 2000). The Xianshuihe–Anninghe Fault forms a natural east boundary of the clockwise rotation (Avouac & Tapponnier 1993; Wang & Burchfiel 2000), while the Jinshajiang-Red River Fault, the LMS Fault and the Xianshuihe–Anninghe Fault separate the region into three main geological units: the Songpan-Ganze (SG) Fold, the Sichuan Basin (SB) and the diamond-shaped SY block. Among these active faults the LMS Fault is the boundary between the SG fold of eastern Tibet and the Sichuan Basin. The Tibetan crust has doubled in thickness as a result of the collision, and a 15–20 km Moho step has formed beneath the LMS (Wang *et al*. 2007, 2009; Zhang *et al*. 2009).

In this section, broad-band data recorded at two permanent stations, XCH and MDS, are processed for a total of 110 teleseismic events with $M \geq 6.2$ and epicentral distances between 30° and 95°. Among the 110 events, a total of 77 receiver functions for XCH and a total of 99 receiver functions for MDS have been selected, based on high signal-to-noise ratio. The location of the stations and seismic events are shown in Fig. 3. The receiver functions beneath each station are obtained using the method developed by Ammon *et al*. (1990). To enhance the converted and reverberated phases, the receiver functions are corrected to a reference slowness of 6.4 s deg^{-1} (corresponds to an epicentral distance of 67°) using IASP91 model and then are stacked.

Moveout correction can be applied to either the *Ps* or the *PpPs* phase. After the *Ps* moveout correction, all *Ps* would be almost paralleled to the direct *P*, but the *PpPs* would be inclined, so that the *Ps* phase is enhanced but the *PpPs* would exhibit a wide biased slope. In contrast, the moveout correction based on the *PpPs* phase results in that the *Ps* phase still have a narrow slope, so that the time delays for both phases can be picked up at one time, without seriously degrading the arrivals. The reference distance of 67° likely equalizes the effect of the events in a range of 30° to 95°.

To obtain the value of $S(H, k)$ in eq. (9), the *H-k* algorithm is applied to the individual receiver functions first, and then the *S(H,k)* for the individual receiver functions is stacked in the *H-k* space to construct the solution surface. For the *H-k* algorithm, we do not conduct any moveout corrections to the individual receiver functions, because principally, the *H-k* doesn't require moveout correction. Figs 4 and 5 are the receiver functions (after the *PpPs* moveout correction) and the solution surfaces (without moveout correction) constructed by the *H-k* for XCH and MDS, respectively.

As shown in Fig. 4(a), the individual receiver functions recorded at station XCH are displayed randomly. Because the station is located in a complex tectonic region, the converted phases are complex in the individual traces. There exist two converted phases in the crust. One appears approximately at 4 s and the other at 6 s. Moreover, the reverberation phases *PpPs* and *PsPs* at the Moho are unclear. In this situation, it is difficult to identify the *Ps* converted phase from the Moho at once. By analysis of the individual traces, we find that two phases, occurring at 27.04 s and 28.6 s, respectively, may be related to the *PpPs* phase from the Moho. If the reverberation phase *PpPs* from the Moho occurs at 27.04 s, the value of t_{Ps}–t_P predicted from eq. (5) should range from 7.55 s to 9.03 s. Thus it might be reasonable to pick the phase at 7.8 s in the stacked trace as the *Ps* from the Moho. However, because the number of traces with *PpPs* phase at 28.6 s is dominant, we prefer the phase at 28.6 s as the *PpPs* phase from the Moho, though its amplitude is weak

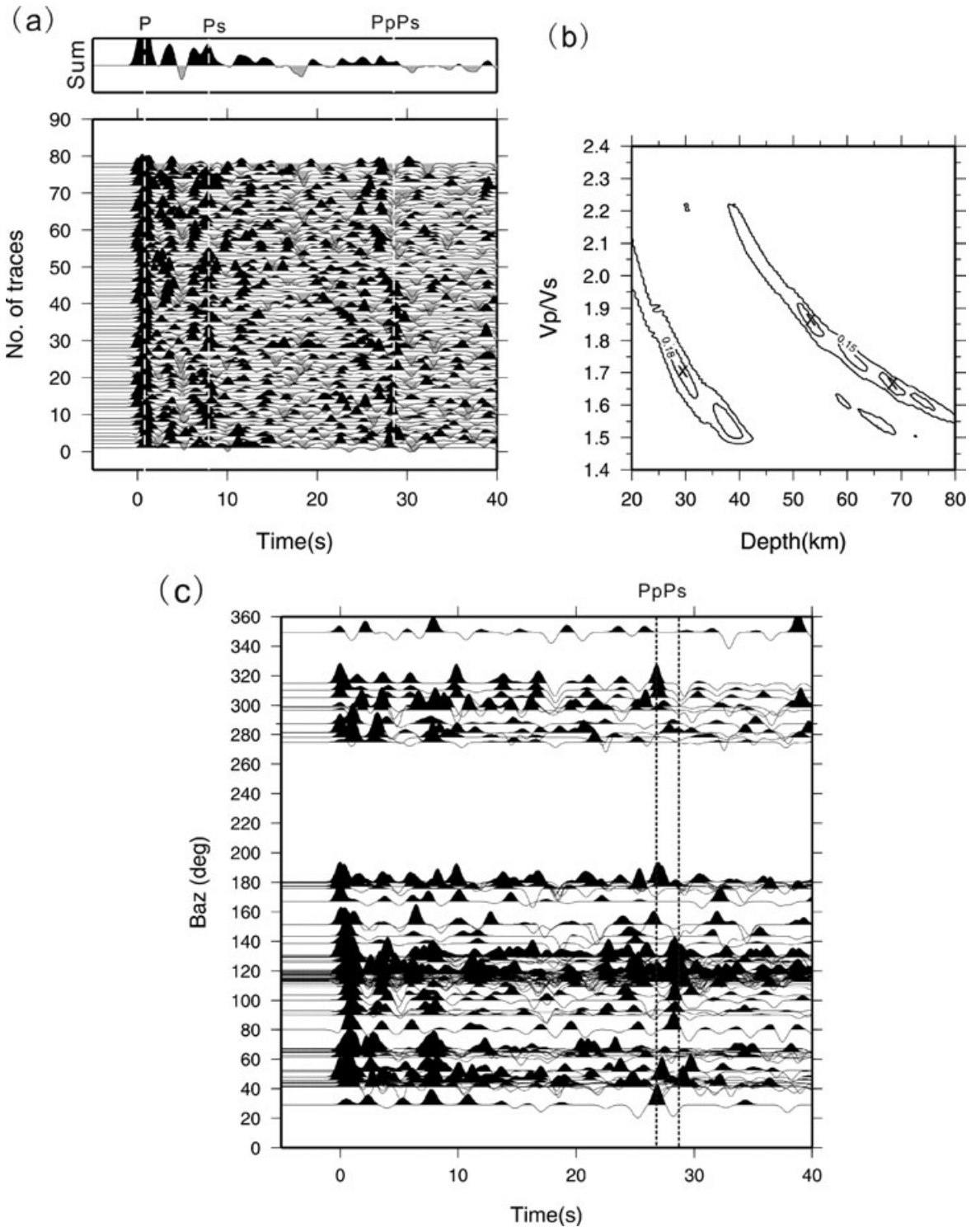

Figure 4. (a) The receiver functions recorded at station XCH, ordered randomly. The top panel is the stacked receiver function, with the phases of *Ps* and *PpPs* from the Moho labelled. (b) The solution surface constructed by the *H-k* algorithm, with the contour intervals at 0.03 and the optimum solution indicated by a cross. (c) The receiver functions arranged according to backazimuth.

in the stacked receiver function. The cause for the weakening may be the lateral structure variation such as a dipping Moho. Though there is a stronger phase before this phase in the stacked trace, we don't think it is the reverberation from the Moho because it exists in only a few individual traces. If the time delay of the *PpPs* phase from the Moho occurs at 28.6 s, the value of $t_{Ps} - t_P$ predicted from eq. (5) should range from 7.7 s to 9.2 s. Finally, we pick the phase occurring at 7.84 s as the *Ps* converted phase from the Moho, and compute the V_p/V_s ratio to be 1.723 using eq. (7). These values yield a crustal thickness of 64.0 km based on eq. (1). On the other hand, the *H-k* algorithm is applied to process the individual receiver functions, and then the solution surface is constructed by stacking the individual $S(H, k)$ surfaces. As shown in Fig. 4(b), the maximum value 0.197 occurs at two points, (53.0, 1.86) and (68.0, 1.66) in

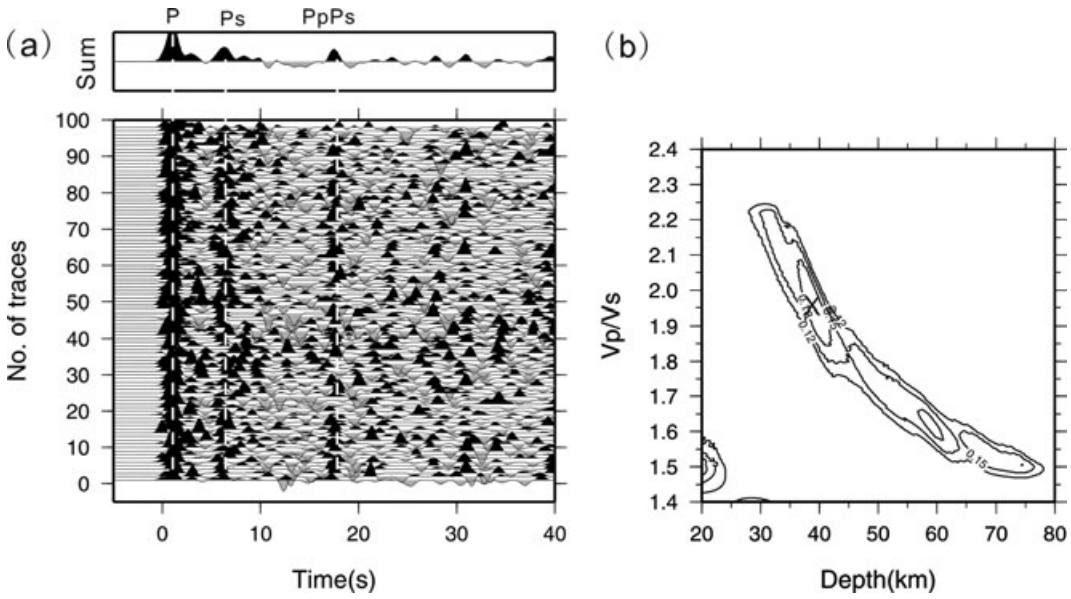

Figure 5. Same as Fig. 4 except for station MDS.

the *H-k* space, respectively. Another extreme value 0.195 occurs at point (30.0, 1.70). Since the three amplitudes are so close, it is difficult to select the optimum solution without knowledge of the tectonic background. To keep consistency with the result from the time delays method, we eventually select the point (68.0, 1.66).

To investigate the cause for the azimuthal variation in the arrival times, that is, due to velocity anisotropy or a dipping Moho, we arrange the receiver functions of station XCH according to the backazimuths of seismic events (Fig. 4c). For the traces having backazimuths from 80° to 140°, the reverberation phase *PpPs* has an arrival time of 28.6 s, while for those traces having backazimuths from 0° to 80° or from 140° to 360°, the reverberation phase *PpPs* has an arrival time approximately at 27.04 s. If it were caused by the velocity anisotropy, the arrival of the *PpPs* in the northwest direction would have been slower as that in the southeast direction, which is not the case. Because there is no events with backazimuth from 180° to 270°, we tentatively infer the difference is likely to result from a southeastward dipping Moho.

Xu *et al*. (2007) used data from a network of 25 temporary broad-band seismometers, and applied the *H-k* algorithm to obtain the crustal thickness and the V_p/V_s ratio in the region. Station MC06 in their study is at the same location as our station XCH. The crustal thickness and the V_p/V_s ratio are 64.0 km and 1.74 in their Table 1, respectively. Their results are very close to ours from the delay-time picking. Reflection profile of Wang *et al*. (2007) and migration imaging of receiver function (Wang *et al*. 2009) have showed that the crustal thickness is approximately 65 km at this location. Our result from the delay-time picking is consistent to their results.

Station MDS is located on the east side of the LMS Fault. As shown in Fig. 5, whether in the individual or stacked waveforms, the *Ps* phase and the *PpPs* phase are clearly visible, occurring at 6.00 s and 18.14 s, respectively, though the phase of *PsPs* + *Pp*Ss from the Moho is invisible in the stacked or individual receiver functions. Moreover, the ratio of the time delays between $t_{PpPs} - t_P$ and $t_{Ps} - t_P$ is 3.02, satisfying eq. (5). The V_p/V_s ratio obtained from eq. (7) is 2.03 and the crustal thickness obtained from eq. (1) is 37 km. The result from the *H-k* algorithm shows that the maximum amplitude is 0.205, occurring at point (39.0, 1.962) in the *H-k* space. Evidently, the results from the *H-k* algorithm and from the time delay are very close. However, we note that there are two optimum solutions on the solution surface, one at depth 40 km and the other at depth 60 km. The second optimum point with amplitude 0.198, is very controversial. Recall that our station MDS is almost at the same location as station MC03 in Xu *et al*. (2007). Similar to our study, Xu *et al*. (2007) described two velocity discontinuities, one at 44 km and the other at 64 km. They concluded that at this location, the crust is a double-layer structure, and the depth of the Moho should be 64 km. Probably, the second optimum solution was selected as the Moho in their article. In contrast, we believe that the first optimum solution is more reliable as the Moho, because (1) previous results (Wang *et al*. 2007, 2009; Zhang *et al*. 2004) have shown that the depth of the Moho becomes dramatically reduced by 15 to 20 km across the LMS Fault; (2) according to the individual receiver functions and the stacked function, the *Ps* and *PpPs* phases resulting from the first discontinuity are very clear, and the time delay satisfies eq. (5); (3) from Fig. 3, station MDS is within the Sichuan Basin, and its crust should be significantly thinner than that of station XCH that is located in the eastern Tibet. In a quick summary, we believe that the depth of the Moho from the delay-time picking is more reliable, while Xu *et al*. (2007) chose the depth of the Moho according to the second optimum on their *H-k* surface.

4 DISCUSSION

Advantages of the *H-k* algorithm include (1) large amount of teleseismic waveforms can be conveniently processed; (2) there is no need to pick arrival times of different phases; (3) through stacking receiver functions from different distances and directions, the effect from lateral variation is statistically suppressed and thus an averaged crustal model is obtained; and (4) uncertainties can be estimated from the flatness of $S(H, k)$ at the maximum. However, if a complex structure exists in the crust, the reverberated phases from different depths will be lain over, resulting in reduction or even absence of the *PpPs* and *PsPs* phases from the Moho. In this situation, multiple points with the maximum amplitude may occur at the solution surface constructed by the *H-k*, and determination of the optimum solution would become ambiguous without *a priori*

knowledge of the tectonic background beneath the station. Once the incorrect point in the *H-k* space is selected, it may result in a significant error. In contrast, determination of crustal thickness and V_p/V_s ratio using the delay-time picking is not sensitive to the crustal *P* velocity, and the computational accuracy depends only on the time delays of the *Ps*, *PpPs* and *PsPs* phases.

The velocity model in Table 1 is a special case, in which the *PLs* phase converted at the LAB is purposely designed to arrives simultaneously with the *PpPs* phase from the Moho, such that the positive *PpPs* phase from the Moho is too weak to identify due to the negative *PLs* phase, causing that the optimum solution cannot be determined by the *H-k*. In reality, the phase of LAB in receiver function is usually too weak to interfere crustal phases, because LAB is usually a diffusion boundary instead of a sharp one as Moho. More likely, the interference between Moho and intracrustal discontinuity which are close to each other on *H-k* space might be the real trouble.

Although we only analysed two stations, in which the optimum solution is difficult to resolve using the *H-k* method, it is believed that other researchers may encounter the similar problem, especially in collision regions such as eastern Tibet. Advantage of the time delays method is that once a converted phase is identified, the arrival times of other phases can be predicted approximately through eqs (5) and (6), such that we can pick up the other conversions accurately and compute crustal depth and velocity ratio stably.

Generally, the phases later than the primary converted *Ps* have tripled or more travel paths through crust than the primary conversion. Therefore, they are more sensitive to lateral structure variation such as a dipping Moho, or are more dispersed on the time axis. A simple stacking of receiver functions from different directions may smear the lateral variation. Moreover, it is easier for the multiple phases to be smeared/dispersed than the primary conversion phase. Generally, in a complex tectonic area such as eastern Tibet, the Moho depth should be investigated by stacking traces according to azimuth. Nonetheless, constrained by the number of events and the distribution of azimuths, that would be a difficult task.

To date, there are a total of 51 permanent broad-band stations deployed in eastern Tibet and Sichuan Basin, which makes it possible to determine the distribution of the crustal thickness and velocity ratio in this region. A total of 5080 receiver functions, resulting from 110 teleseismic events with $M \geq 6.2$ and epicentral distances between 30° and 95°, are obtained. For each station, the receiver functions are moveout corrected to a reference slowness of 6.4 s deg^{-1} and are stacked, and then the time delays method is applied to extract the depth of the Moho and the velocity ratio from the stacked receiver functions. The *H-k* algorithm is also applied to obtain the depth of the Moho and the velocity ratio. For the purpose of comparing the results, we first plot the contour maps of the thickness and the crustal Poisson's ratio resulting from a direct picking of the maximum on the solution surface; see Figs 6 and 7. In Fig. 6, the crustal thickness changes dramatically. The crust thickness in the SY block is as low as to 24 km. On the western Sichuan Basin, the depth of the Moho is as high as 72 km. It appears to be unlikely that the crust thickness is tripled on a length scale of about 200 km. At this location, the LMS Fault, the Xianshuihe–Anninghe Fault and the Lijiang–Jinhe Fault converge and the crustal structure is pretty complicated. Especially, due to the collision between the Eurasian plate and the Indian plate, crustal material from Tibet extrudes eastwards and southeastwards. This extrusion should be accommodated by a thickening crust. The interface at depth 24 km is very likely an intracrust one. Additionally, the crustal Poisson's ratio in Fig. 7 reaches as low as to 0.21 ∼ 0.24, which is unrealistic because according to Zandt *et al*. (1995), the crustal Poisson's ratio cannot reach such a low value, especially in a tectonic-active area where fluids are present in the crust. Though the Sichuan Basin is a rigid and cold block, its sedimentary layer reaches deep into 5 to 10 km. Therefore, the ratio could not be so low. This result is attributed to simple selecting the maximum on the solution surfaces constructed by the *H-k* without considering the tectonic background.

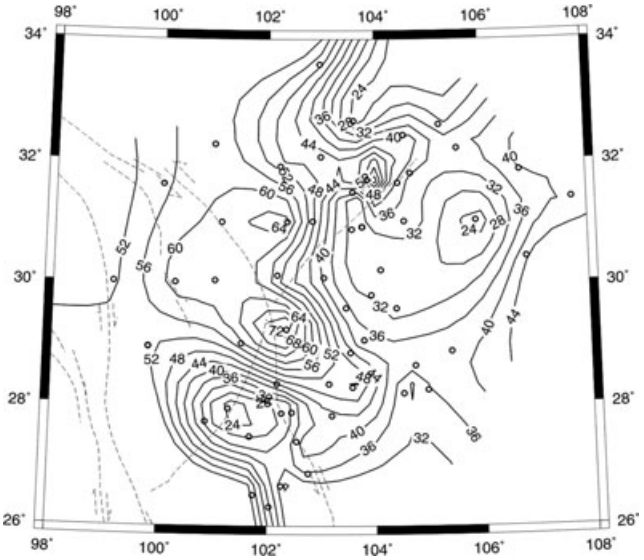

Figure 6. The contour map of the crustal thickness (in kilometres) obtained directly from the first maximum on the solution surface constructed by the *H-k* algorithm, with the circles representing the stations and the dash lines denoting the faults.

For avoiding the above unrealistic results, we now use a mixed optimal method to determine the crustal thickness and the Poisson's ratio. With this method, we select the optimal solution when there are several extremes on the solution surface, considering consistency with the crustal thickness from the time delays method. The crustal thickness and the Poisson's ratio from this mixed optimal method and from the time delays method are plotted, respectively, in Figs 8 and 9. Compared with the result from the direct *H-k*, the result from the mixed optimal *H-k* is improved and more realistic. In

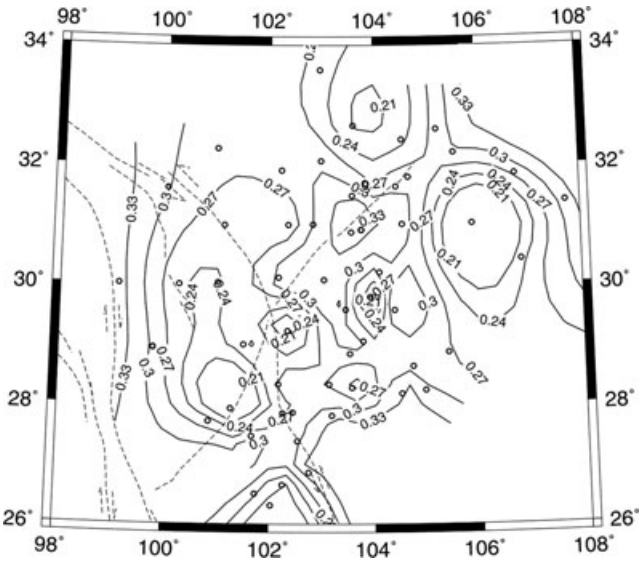

Figure 7. Same as Fig. 6 except for the crustal Poisson's ratio.

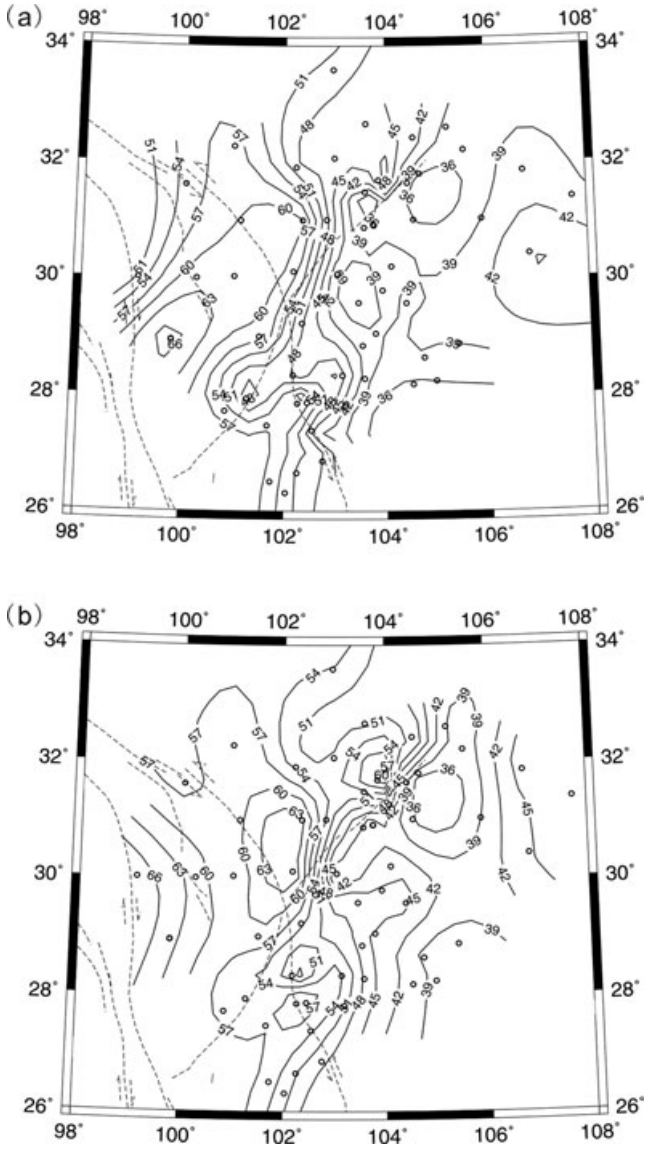

Figure 8. The contour map of the crustal thickness (in kilometres) in eastern Tibet obtained from the receiver functions, with the circles representing the stations and the dash lines denoting the faults: (a) from the mixed optimal *H*-*k*, (b) from the time delays.

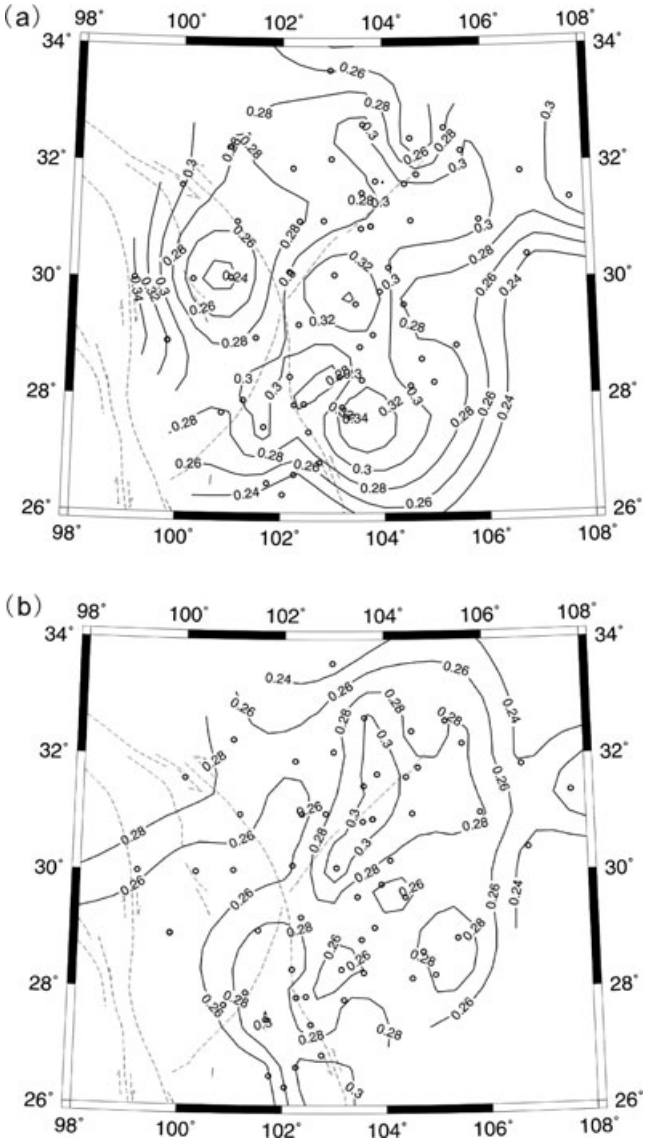

Figure 9. Same as Fig. 8 except for the crustal Poisson's ratio.

Fig. 8, the crustal thickness from the optimal *H*-*k* method is close to that from the time delays, except at eastern Himalayan syntaxis where the thickness from the *H*-*k* is significantly thinner than that from the time delays. Previous sounding profile (Wang *et al*. 2007) and receiver function imaging (Wang *et al*. 2009) have verified that the crustal thicknesses ranges from 60 to 70 km in this area. Therefore, the result from the time delays is believed to be more accurate.

Although the mixed optimal *H*-*k* has accounted the consistency with the time delays method in the crustal thickness when selecting the extremes, the Poisson's ratio, as showed in Fig. 9, has significant discrepancy locally, especially in the Sichuan Basin. In the central Sichuan Basin, the crustal Poisson's ratio from the time delays ranges from 0.26 to 0.28, while that from the mixed optimal *H*-*k* is from 0.28 to 0.32. The previous works suggest that the basin is a rigid block of Yangzi Craton (Lebedev & Nolet 2003; Copley & McKenzie 2007), and the crustal Poisson's ratio should be small. In this sense, the result obtained by the mixed optimal *H*-*k* is not consistent with the geological background.

GPS measurements have confirmed that crustal material is moving eastwards in eastern Tibet (Zhang *et al*. 2004) and is obstructed by the rigid Sichuan Basin of the Yangtze Craton (Copley & McKenzie 2007). Accordingly, the LMS Fault is interpreted as the result of middle/lower crust flow from Tibet thrusting upwards and accumulating there. Therefore, more fluids should be present under the LMS than on its two sides, such that the crustal Poisson's ratio under the LMS is higher than those on the two sides, as observed by Zhang *et al*. (2009) and Wang *et al*. (2009). In Fig. 9, the crustal Poisson's ratio under the faults from the time delays is higher than those on the two sides, which is surprisingly consistent with the physical process and the previous results. Unfortunately, the Poisson's ratio under the LMS Fault and the Xianshuihe Fault from the mixed optimal *H*-*k* does not reveal such a feature yet.

5 CONCLUSIONS

In summary, when the converted phases or reverberation phases from the Moho are reduced and absent in receiver functions, mul-

tiple extremes would appear on the solution surface constructed by the *H-k* algorithm (in which case the optimum solution is difficult to select). In area with complex tectonics, there may be one or several interfaces within the crust, such that multiple extrema may appear on the solution surface. Though we only analysed the results of two stations out of 51 stations, other stations may suffer from the same problem. Figs 6 and 7 from the direct *H-k* present misleading results. Though the mixed optimal *H-k* produces an improved result than the direct *H-k* in the crustal thickness, the Poisson's ratio is still inconsistent with the physical process (i.e. middle/lower crust flow from Tibet thrusting upwards and accumulating there) and the tectonic background under the LMS Fault and the Xianshuihe Fault (i.e. more fluids present under the faults than on the two sides). Through comparing the Moho depth and the crustal Poisson's ratio in eastern Tibet and Sichuan Basin from three methods, that is, the direct *H-k*, the mixed optimal *H-k*, and the time delays, it is concluded that in area having complex tectonics, identifying the converted and reverberated phases based on eqs (5) and (6), and then picking up their time delays is more reliable for determining these two parameters.

ACKNOWLEDGMENTS

This research was sponsored by the National Science Foundation of China under contract U0933602. The authors sincerely thank the Editor, Prof. Randy Keller, and two anonymous reviewers for their insightful comments and constructive suggestions.

REFERENCES

Ammon, C.J., Randall, G.E. & Zandt, G., 1990. On the non-uniqueness of receiver function inversions, *J. geophys. Res.,* **95**, 15 303–15 318.

Avouac, J.P. & Tapponnier, P., 1993. Kinetic model of active deformation in central-Asia, *Geophys. Res. Lett.,* **20,** 895–898.

Bostock, M.G., 1998. Mantle stratigraphy and evolution of the Slave Province, *J. geophys. Res.,* **103,** 21 183–21 200.

Bostock, M.G., Hyndman, R.D., Rondeny, S. & Peacock, S.M., 2002. An inverted continental Moho and serpentinization of the forearc mantle, *Nature,* **417,** 536–538.

Clark, M.K. & Royden, L.H., 2000. Topographic ooze: building the eastern margin of Tibet by lower crustal flow, *Geology,* **28,** 703–706.

Copley, A. & McKenzie, D., 2007. Model of crustal flow in the India-Asia collision zone, *Geophys. J. Int.,* **169,** 683–698.

Gurrola, H., Baker, G.E. & Minster, J.B., 1995. Simultaneous timedomain deconvolution with application to the computer of receiver functions, *Geophys. J. Int.,* **120,** 537–543.

Kennett, B., 1983. *Seismic Wave Propagation in Stratified Media,* Cambridge University Press, Cambridge.

Kind, R. *et al*., 2002. Seismic images of the crust and upper mantle beneath Tibet: evidence for Eurasian plate subduction, *Science,* **298,** 1219–1221.

King, R.W. *et al*., 1997. Geodetic measurement of crustal motion in southwest China, *Geology,* **25,** 179–182.

Langston, C.A., 1979. Structure under Mount Rainier, Washington, inferred from teleseismic body waves, *J. geophys. Res.,* **84,** 4749–4762.

Lebedev, S. & Nolet, G., 2003. Upper mantle beneath Southeast Asia from S velocity tomography, *J. geophys. Res.,* **108**, 2048, doi:10.1029/2000JB000073.

Wang, E. & Burchfiel, B.C., 2000. Late Cenozoic to Holocene deformation in southwestern Sichuan and adjacent Yunnan, China, and its role in formation of the southeastern part of the Tibetan Plateau, *Geol. Soc. Am. Bull.,* **112,** 413–423.

Wang, C.Y., Han, W., Wu, J., Lou, H. & Chan, W.W., 2007. Crustal structure beneath the eastern margin of the Tibetan Plateau and its tectonic implications, *J. geophys. Res.,* **112,** B07307, doi:10.1029/2005JB003873.

Wang, C.Y., Lou, H., Silver, P.G., Zhu, L. & Chang, L., 2009. Crustal structure variation along 30° N in the eastern Tibetan Plateau and its tectonic implications, *Earth planet. Sci., Lett.,* **289**(2010), 367–376.

Xu, L., Rondenay, S. & van der Hilst, R.D., 2007. Structure of the crust beneath the southeastern Tibetan Plateau from teleseismic receiver functions, *Phys. Earth planet. Inter.,* **165,** 176–193.

Zandt, G. & Ammon, C.J., 1995. Continental-crust composition constrained by measurements of crustal Poisson ratio, *Nature,* **374**(9), 152–154.

Zandt, G., Myers, S.C. & Wallace, T.C., 1995. Crust and mantle structure across the Basin and Range-Colorado Plateau boundary at 37° N latitude and implications for Cenozoic extensional mechanism, *J. geophys. Res.,* **100,** 10 529–10 548.

Zhang, P.Z., Shen, Z., Wang, M. & Gan, W., 2004. Continuous deformation of the Tibetan Plateau from Global Positioning System data, *Geology,* **32,** 809–812, doi:10.1130/G20554.1.

Zhang, Z., Wang, Y., Chen, Y., Houseman, G.A., Tian, X., Wang, E. & Teng, J., 2009. Crustal structure across Longmenshan fault belt from passive source seismic profiling, *Geophys. Res. Lett.,* **36,** L17310, doi:10.1029/2009GL039580.

Zhu, L.P. & Kanamori, H., 2000. Moho depth variation in southern California from teleseismic receiver functions, *J. geophys. Res.,* **105**(B2), 2969–2980.